Passive approach to expand the field of view of receivers for free-space laser communications

Yoshihisa Takayama
Werner Klaus
Keisuke Shinohara*
National Institute of Information and Communications Technology
4-2-1 Nukui-Kita, Koganei, Tokyo 184-8795 Japan
E-mail: takayama@nict.go.jp

Abstract. We present an unconventional approach to passively expand the field of view of optical receivers for free-space laser communications. The illumination area, given by the movement of a focused light spot due to different angles of reception, is reduced to a smaller area without expanding the propagation angle of the spot. The working principle of this approach is based on combining a photonic crystal's negative refractive behavior with properly bent crystal boundaries. The device's optical behavior is determined by means of rigorous electromagnetic computation, but the overall working principle of illumination area reduction can be well visualized by the ray trace method. In addition, we estimate the influence of light modulation for high-speed data transmission. Since the discrete structure of photonic crystals only approximates a bent boundary with an arbitrary inclination angle, a slight modification is introduced into the crystal's structure to enable a more flexible design. Although such a modification influences the negative refractive behavior, the function of field-of-view expansion is still verified and confirmed by means of electromagnetic computation. [DOI: 10.1117/1.1911015]

Subject terms: micro-optics; optical communications; optical devices.

Paper 040383 received Jun. 17, 2004; revised manuscript received Nov. 30, 2004; accepted for publication Dec. 6, 2004; published online May 12, 2005.

1 Introduction

In a free-space laser communication system, dynamic variations of an optical terminal's relative positions and dynamic wavefront distortions of the optical beam make it difficult to obtain a low-error-rate data transmission. For instance, a temporal change in the propagation angle causes the focal spot to move across the detector's active area. Such an increase in the illumination area decreases seriously the efficiency of beam detection if the spot falls momentarily outside the detector's active area. The simplest method to counteract this enlargement of the illumination area is to use a lens of shorter focal length. However, by using only conventional optics, the more one tries to reduce the beam's illumination area, the more one also expands its angular spectrum. Such an expansion in the propagation angle brings about another type of optical loss due to the limitation in the receiver's detectable angular range, i.e., its numerical aperture, which becomes important if for instance the light must be coupled to a fiber. To avoid the expansion in the propagation angle, a reduction of the illumination area must be performed by active methods involving wavefront sensors and wavefront correctors such as arrayed detectors and motion-controlled mirrors.[1,2] These methods stabilize the location of the focal point and thus enhance coupling efficiency.

Recently, the anomalous optical properties of photonic crystals have attracted a lot of attention. It is known that one can design the structure of photonic crystals in such a way that beams at specific wavelengths do not propagate at all, or that beams inserted simultaneously from several input angles can be forcibly aligned to propagate only along a single direction within the crystal.[3–6] In this paper, we concentrate on the negative refractive behavior exhibited by photonic crystals and work on a passive method to reduce the resultant focal illumination area while conserving the propagation angles of light. One application area we look at is free-space laser communications, where our device can act as a field-of-view expander for optical receivers. The key to obtaining this expansion lies in the combination of a properly designed photonic crystal structure and crystal surfaces interfacing with air. With such a device, the optical setup becomes as simple as the one using a fast lens, but the provided function is similar to that of active methods.[7]

First, we show the fundamental idea of our approach with a sample crystal whose optical behavior is predicted by the dispersion diagram and the constant-frequency plot. These predictions, which are based on the assumption of a theoretically infinite structure, are confirmed by rigorous electromagnetic analysis using the Fourier modal method[8] (FMM) applied to a more realistic finite structure. Using the optical characteristics obtained from the constant-frequency plot, we then estimate the performance of the reduction in the illumination area with the ray trace method, where the preservation of propagation angles of the incoming beams is confirmed as well. We additionally consider the case of data transmission in a free-space laser communication, where we should expect a spread of wavelength range due to modulation of light. Since the optical characteristics of photonic crystals are strongly dispersive and thus sensitive to the illumination wavelength, we fur-

*Keisuke Shinohara is presently with Rockwell Scientific Company LLC, 1049 Camino Dos Rios, Thousand Oaks, California 91360.

0091-3286/2005/$22.00

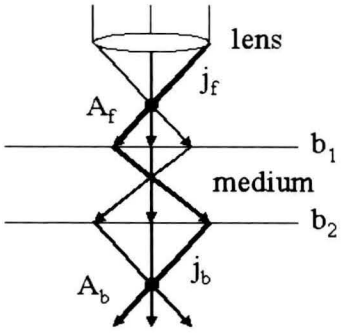

Fig. 1 Propagation of light through a medium exhibiting negative refraction. The focal point A_f is reproduced at the point A_b behind the slab. The bold arrow labeled j_f is parallel to the arrow j_b when the boundaries b_1 and b_2 are mutually parallel.

ther investigate the reduction in the illumination area with respect to the modulation rate in a digital transmission assuming intensity modulation methods. Finally, we briefly discuss some fabrication methods and the influence of structural misalignment in the crystal.

In general, the structure of photonic crystals is discrete because of the periodic arrangement of different dielectric materials in form of a lattice. Therefore, a standard approach to approximate a bent boundary would be the use of a stairlike interface. To bring the approximated boundaries closer to the expected ones, we introduce a slight modification in the arrangement of the crystal's lattice. Although such a modification enables us to design arbitrary crystal boundaries, it also causes a slight change in the optical characteristics of the crystal. Such a modification influences the negative refractive behavior of the crystal, but the function as a field-of-view expander was still confirmed by using the finite-difference time-domain (FDTD) method.[9]

2 Reduction of Illumination Area

It is well known that when a slab consisting of a medium with negative refractive index is placed behind a lens, as shown in Fig. 1, it causes[10] the rays exiting from focal point A_f to gather again at the point A_b. For example, the ray denoted by the bold arrow labeled j_f goes into the slab from air, refracts toward a negative direction in the angular sense, and finally exits as the ray labeled j_b. When the boundaries of the slab b_1 and b_2 are mutually parallel, the arrows j_f and j_b point in the same direction. Therefore, an optical detector accepting light at position A_f can be replaced by one positioned at A_b to receive the light within the same numerical aperture. Here we note that the line connecting the points A_f and A_b is perpendicular to the boundaries b_1 and b_2.

This line of thought led us to consider an approach shown in Figs. 2(a) and 2(b). Figure 2(a) shows temporal variations in the propagation angle of light received by a lens or telescope during free-space laser communications. We observe the focal spot A_{f1} at t_1, but it moves to A_{f2} at t_2 and A_{f3} at t_3 due to different wavefront tilts, where the focal plane locates in front of a medium with bent boundaries interfacing to air. According to the negative refractive behavior shown in Fig. 1, every ray penetrating the medium gathers again behind the medium at the locations denoted

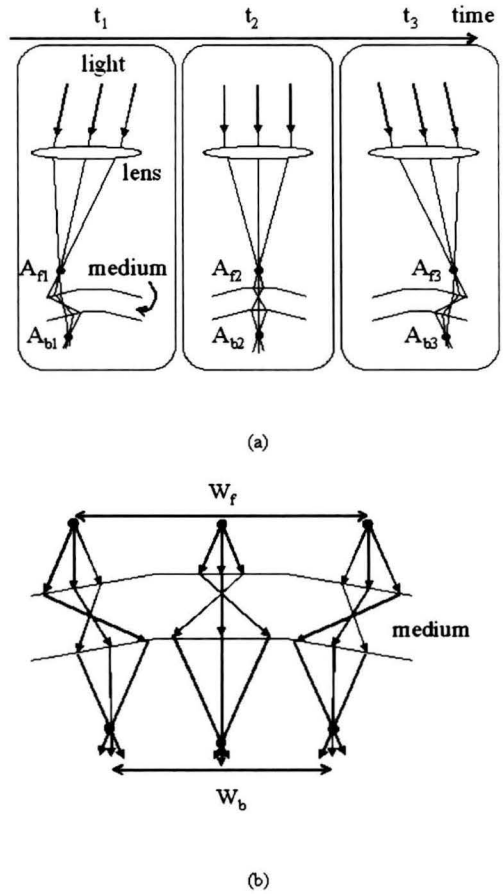

Fig. 2 Reduction of illumination area: (a) temporal variation of propagation angle of light coming to a lens, where each focal spot of the lens A_{fi} is reproduced at A_{bi} (i=1,2,3), and (b) the whole illumination range of received light W_f in front of a medium with bent boundaries reduced to the range W_b but with the propagation angles conserved.

by A_{b1}, A_{b2}, and A_{b3}, respectively. Thus, the whole illumination range W_f on the focal plane is reduced to W_b, as shown in Fig. 2(b). But the propagation direction of each ray in front of and behind the medium remains the same if the boundaries in each case are mutually parallel. Therefore, even if the diameter of an optical detector is smaller than W_f, all the rays can enter the detector if the detector with a larger diameter than W_b is put behind the device. Figure 3(a) shows a schematic drawing of an optical receiver, where the detectable angular range θ_1 is depicted by the bold lines. The restriction of the detectable angular range is caused by the diameter of a detector. In Fig. 3(b), the diameter of a detector is the same as that shown in Fig. 3(a). But the angular range θ_2 is enlarged by inserting the device between the lens and the detector. Thus, this device works as a field-of-view expander (FOVE) of optical receivers.

3 Design of a Sample

The photonic crystal's 2-D lattice structure is shown in Fig. 4. The rectangular rods with the cross section size $a \times b$ have a rectangular arrangement described by the lattice vectors $\mathbf{l}_1$ and $\mathbf{l}_2$. We assume that $\mathbf{l}_1$ and $\mathbf{l}_2$ are parallel to

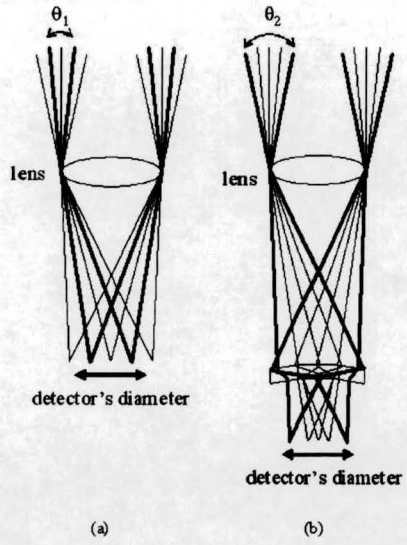

Fig. 3 Schematic drawings of (a) a conventional optical receiver and (b) a receiver with the field-of-view expander. The detectable angular range θ_2 of the received light becomes larger than θ_1 with the same lens.

the x and y axes, respectively, and that they are of the same length d, i.e., they are arranged according to a square lattice. We further assume that the rod and background refractive indices n_r and n_b are 3.35 and 1.55, respectively.

The crystal's dispersion property is calculated by means of the plane wave expansion method.[11–13] Figure 5 shows the dispersion diagram of a photonic crystal with $a=0.1d$ and $b=0.4d$ when the electric field is assumed parallel to the rod axis. The inset indicates the symmetric points in k space, where Γ, X, M, and K denote the points $(k_x,k_y)=(0,0)$, $(\pi/d,0)$, $(\pi/d,\pi/d)$, and $(0,\pi/d)$, respectively. For the evaluation of the optical characteristics, we concentrate on the value $d/\lambda=0.51$, i.e., where the lattice period is about half a wavelength. This is represented by the dashed line in Fig. 5. The constant-frequency plot is shown in Fig. 6(a), where the profiles of the second, third, and fourth lowest bands in Fig. 5 projected on the intersection plane at

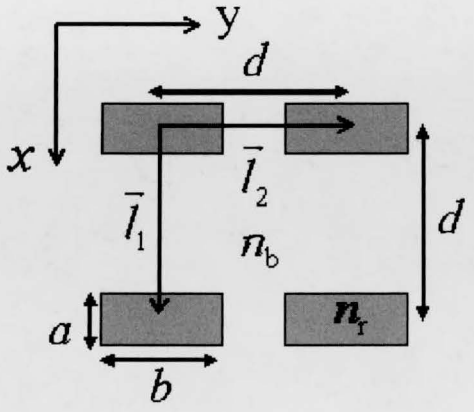

Fig. 4 Cross-sectional view of a photonic crystal's structure. The rectangular rods $a\times b$ are arranged in the square lattice of the side length d. The refractive index of the rods n_r is given as 3.35 and that of the background n_b is 1.55.

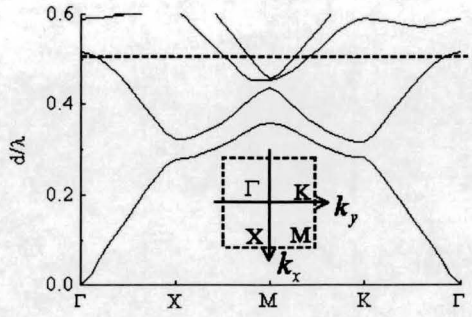

Fig. 5 Dispersion diagram of the photonic crystal. The inset indicates the notation of symmetric points in k space. The dashed line corresponds to $d/\lambda=0.51$.

$d/\lambda=0.51$ are included. Among these profiles, we concentrate on the closed curve centered at $(k_x,k_y)=(0,0)$, which corresponds to the second lowest band in Fig. 5. The optical behavior represented by this band represents negative refraction because the inclination of the second lowest band at the intersection with the dashed line is negative, or in other words, because k decreases with increasing frequency d/λ. Figure 6(b) shows a part of Fig. 6(a) expanded around the origin of k space to look at this closed curve. The shape is viewed as a circle with radius 0.063 in $2\pi/d$ units. When illuminating the crystal from air within the angular range of -7.1 and $+7.1$ deg measured from the normal to the crystal's boundary, the light in the crystal exhibits negative refractive behavior. For instance, if the crystal is exposed to light at an incident angle of 3 deg, the energy flow of the light inside the crystal occurs at -25.1 deg.

The calculation of the dispersion characteristics assumes a crystal lattice of infinite size. Since the real crystal has

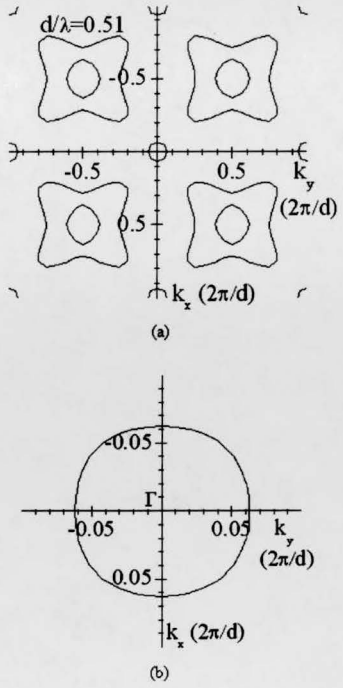

Fig. 6 (a) Constant-frequency plot at $d/\lambda=0.51$, where the center circle corresponds to the second band in Fig. 5, and (b) the circle expanded around point Γ. The radius is 0.063 in $2\pi/d$ units.

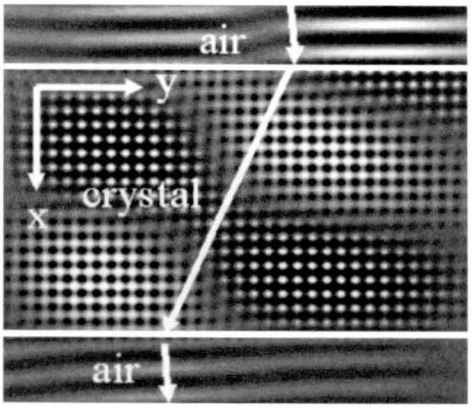

Fig. 7 Electric field distribution computed by FMM. The Gaussian beam illuminates the crystal at 3 deg measured from the normal to the boundary.

boundaries with air, the validity of the calculation needs to be confirmed. For this confirmation, we employ the electromagnetic computation of the FMM. The computed result is shown in Fig. 7, where the crystal's parameters are those from Figs. 4 to 6 and with a crystal thickness of 20 layers. The crystal's boundary with air is parallel to the y direction and illuminated with a light propagating at 3 deg measured from the normal to the crystal's boundary. According to Fig. 7, light inside the crystal propagates at an angle of around -25 deg. Thus, it is reasonable to assume that the refractive behavior of the light illuminating the crystal can be predicted by the dispersion diagram and the constant-frequency plot with sufficient precision.

Next, we assume that the crystal has curved boundaries and look at three points A, B, and C within the width W_f at $x=0$ in front of the crystal. As shown in Fig. 8 we then employ the ray-trace method to visualize the propagation directions of light through and behind the crystal. The distances between A and B, and B and C, are normalized to 1. The boundaries b_1 and b_2 are segments of circles with the same center. In our evaluation, the normalized radii b_1 and b_2 amount to 30 and 28, respectively. The result in Fig. 8 is shown with an expanded scale in the y direction where the reduction of illumination area can be observed. The minimum width W_b through which all the rays penetrate is 37.5% of W_f obtained at $x=18.9$. In addition, we plotted the propagation angles of each ray inside the crystal in Fig. 9(a) and those behind the crystal in Fig. 9(b). Although the propagation angle inside the crystal is relatively large, the

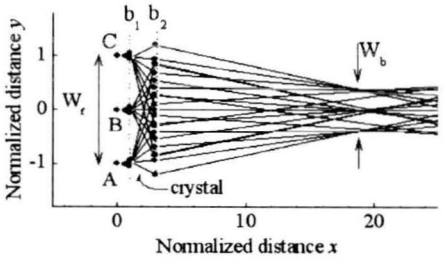

Fig. 8 Ray-tracing result. The minimum width W_b through which all the rays passes is 37.5% of W_f at $x=18.9$.

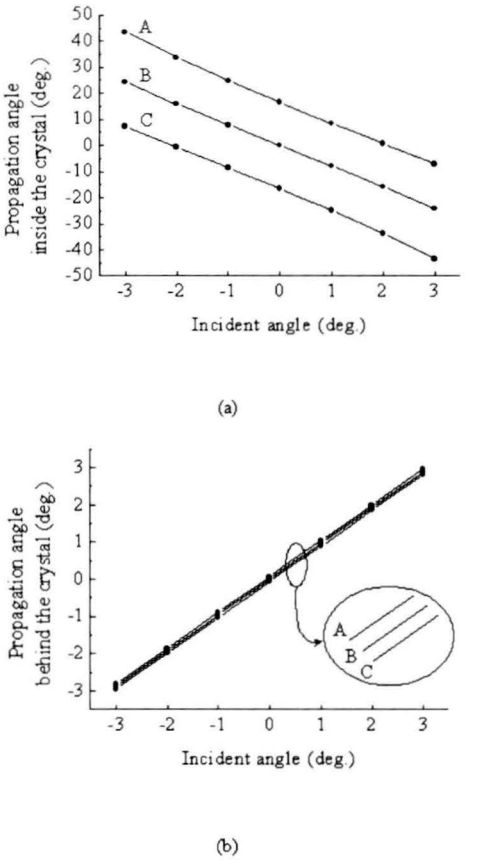

Fig. 9 Propagation angles of rays (a) inside the crystal and (b) behind the crystal. The angles behind the crystal are almost equal to those of incident beams.

angle behind the crystal becomes almost equal to that in front of the crystal. As a result, we consider that the requirements of reduction of illumination area with no expansion in propagation angle can be achieved by this approach.

4 Influence of Light Modulation

Although we have assumed monochromatic illumination of the photonic crystal, modulation of light for data transmission spreads the wavelength range in practical situations. Since the optical characteristics of photonic crystals are sensitive to the wavelength of exposure, it is important to estimate the influence of such a modulation on the performance of the reduction in illumination area. Here we assume a digital transmission by intensity modulation methods. The top of Fig. 10 is a part of a pseudorandom sequence of 0's and 1's. The middle and the bottom of Fig. 10 show two popular forms of modulation such as non-return-to-zero (NRZ) and return-to-zero (RZ), respectively. When the wavelength of the carrier is given as 1550 nm, the parameters of the photonic crystal in Fig. 4 are determined to be $d=790.5$ nm, $a=79.05$ nm, and $b=316.2$ nm. The power distribution of the modulated light is shown in Figs. 11(a) and 11(b), assuming a data rate of 40 Gbits/s. The arrow in each figure denotes the wavelength range which contains 99% energy of the transmitted light.

By repeating the calculation of the crystal's dispersion characteristics with respect to wavelengths chosen from

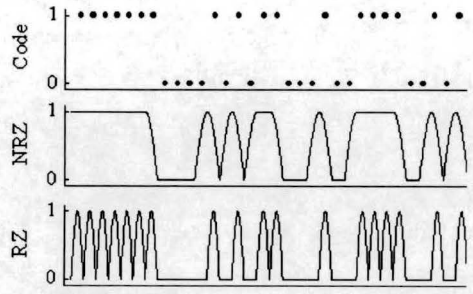

Fig. 10 Part of a quasirandom array with the binary codes of 0 and 1, and the intensity modulations of NRZ and RZ.

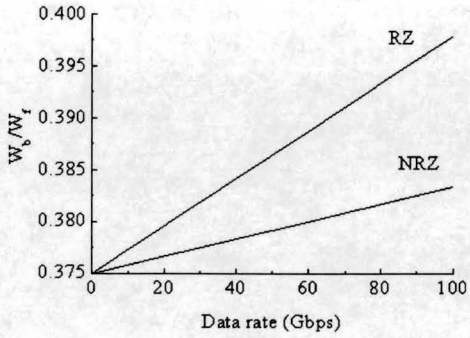

Fig. 12 Influence of intensity modulation on the performance of FOVE.

this wavelength range we obtain the required width through which all the rays pass behind the crystal. The result is shown in Fig. 12, where the value of 0.375 on the ordinate represents the case of no light modulation. Although the performance in area reduction degrades with the increase of the data transmission rate, the width W_b is still less than 38.3% of W_f in the NRZ case and 39.8% of W_f in the RZ case with the data rate up to 100 Gbits/s. Therefore, we conclude that the influence of light modulation on the performance of the reduction in the illumination area is insignificant within today's practical modulation rates.

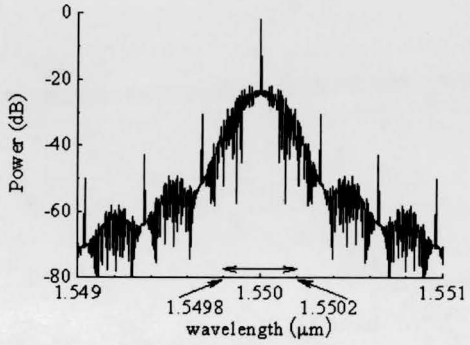

(a)

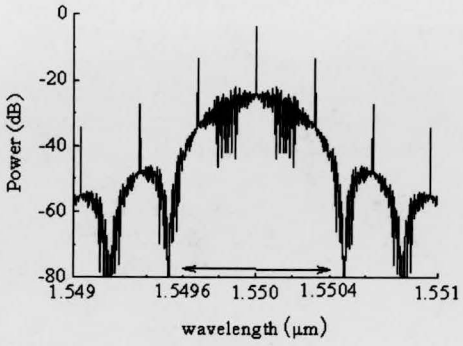

(b)

Fig. 11 Power distribution of light modulated at 40 Gbits/s. 99% energy is contained within the wavelength range denoted by the arrows. (a) RZ case and (b) NRZ case.

5 Modification of the Crystal Structure

The sample calculation shown in Fig. 8 provides a good insight into the behavior of FOVE, however, such bent lines for arbitrary inclination angles can only be approximated in practice due to the discrete structure of the photonic crystal. Figure 13(a) shows the tilted boundary approximated by a discrete structure. The requirement for the validity of this approximation is to make the entire size large enough compared to the size of a unit cell. Another possible approach is shown in Fig. 13(b), where a slight modification is put into the photonic crystal's structure. This approach enables us to design the crystal's boundaries at arbitrary inclination. However, from the viewpoint of the crystal's dispersion characteristics, such a modification simultaneously causes a deformation in the dispersion diagram and the constant-frequency plot.

As an example, we introduce a slight angular shift in the lattice vector $\mathbf{l}_2$ to make an angle ϕ with the y direction and calculate the constant-frequency plot. In Fig. 14, we show the constant-frequency plot corresponding to the second lowest curve shown in Fig. 6, with values of ϕ such as 3 and 5 deg. For comparison purposes we also added the case $\phi=0$. Although the closed curves move gradually away from the circular shape with the increase of the angle ϕ, we can still expect negative refraction. The propagation of light through the photonic crystals computed by the FDTD method is shown in Figs. 15(a) to 15(c), where a Gaussian beam with a beam waist of 4λ illuminates the crystal. The angle ϕ is 0 in the case of Fig. 15(a), i.e., the crystal's

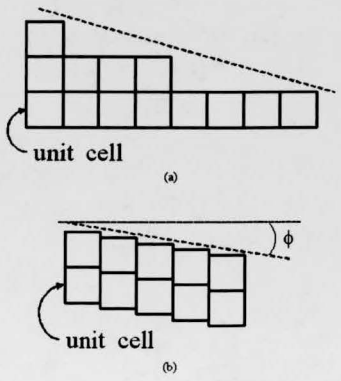

Fig. 13 Bent boundary of a photonic crystal approximated (a) by means of a stair-step profile and (b) by a modified crystal structure.

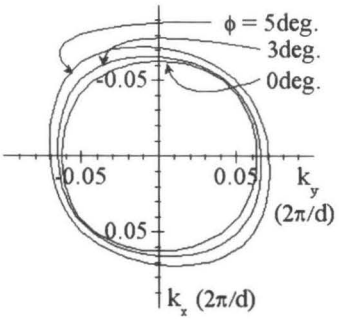

Fig. 14 Deformed constant-frequency plot due to a slight modification of the crystal's structure.

boundaries are parallel to the y direction. As shown in Fig. 1, the light gathers behind the crystal. Figures 15(b) and 15(c) show the cases of $\phi=3$ and 5 deg, respectively. Because of the inclined boundaries introduced by the angular change in the lattice vector, the position at which the light gathers is spatially shifted. Thus a proper modification of the crystal's structure can also be considered to achieving the fundamental concept shown in Fig. 2.

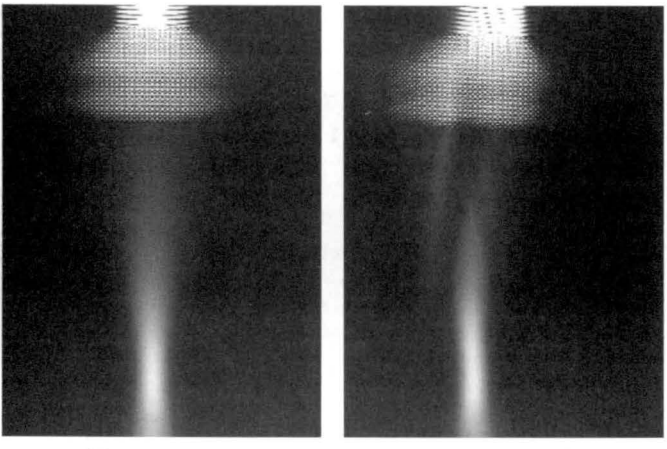

(a) (b)

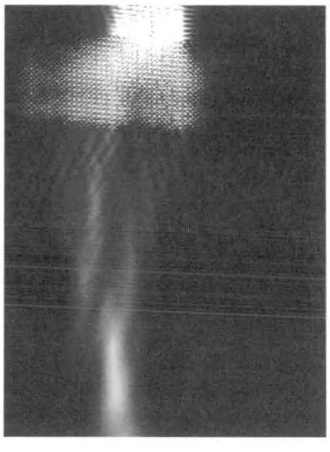

(c)

Fig. 15 Computed result of $|E|^2$ by FDTD method for (a) $\phi=0$ deg, (b) $\phi=3$ deg, and (c) $\phi=5$ deg.

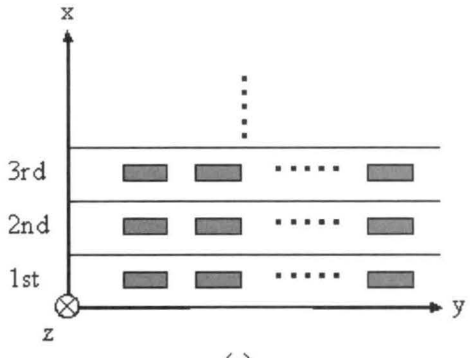

(a)

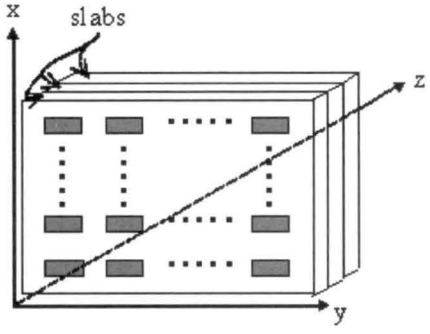

(b)

Fig. 16 Fabrication methods of a photonic crystal where (a) the rod layers lie parallel to the *yz* plane and (b) photonic crystal slabs are in the *xy* plane.

To work efficiently as an FOVE, the photonic crystals extensions should be larger than the area denoted by W_f in Fig. 2. Additionally, a means to enable some modifications in the crystal's structure during the fabrication process is desired. We show two possible approaches for fabrication in Figs. 16(a) and 16(b). In Fig. 16(a), the first layer of a photonic crystal is placed on a base substrate lying in the yz plane. After the first layer is completed, the fabrication process for the second layer begins on top of the first layer. Similarly, the third layer is made on top of the second layer, and so on. Since the light illuminates the crystal's surface in the yz plane, this approach provides an adequate exposure area. But the design of crystal's structure is limited due to such a layer-by-layer process and is suited only for the discrete boundary shown in Fig. 13(a). In Fig. 16(b), thin slabs containing short rods with an arbitrary arrangement in the xy plane are combined along the z axis. This approach also suits the bent boundary shown in Fig. 13(b), but many slabs must be stacked to obtain a large exposure area. A common requirement for both approaches is the accurate alignment of layers.

During fabrication, a small amount of misalignment is almost unavoidable. In the following we therefore briefly discuss the influence of rod misalignment on the negative refractive behavior. In our analysis,[14] we introduced some random misalignment in the lateral position of each layer, as shown in Fig. 17, where Δ_i indicates the amount of shift along the y axis at the i'th layer. The distance between neighboring rods in the lateral direction remains d. The

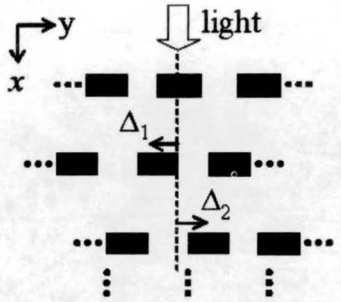

Fig. 17 Schematic drawing of rod misalignment.

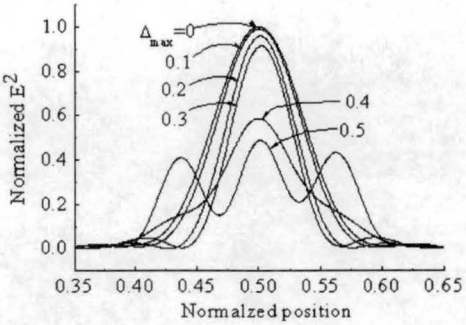

Fig. 19 Degradation of the focusing effect due to rod misalignment.

provided photonic crystal consists of 24 layers with the unit cells as given by Fig. 4. For each layer, a random value is assigned to Δ_i selected from the range of $|\Delta_i| \leq \Delta_{\max}$. The FDTD method is used to simulate the light propagation. Here, we assume that the illumination wavelength is $0.505d$ and the polarization vector of the electric field is parallel to the rod axis. In Figs. 18(a) to 18(c), we show several snap shots of the square of the electric field strength (E^2) when $\Delta_{\max}$, normalized with d, is given as 0, 0.3, and 0.5, respectively. The average and the standard deviation of the misalignment are 0.004 and 0.16 at $\Delta_{\max}=0.3$ and 0.03 and 0.29 at $\Delta_{\max}=0.5$. In Fig. 18(a), the perfectly aligned structure exhibits the focusing effect. However, an increase of $\Delta_{\max}$ starts to degrade the crystal's performance, as shown in Figs. 18(b) and 18(c). For comparison, we normalize the maximum amplitude behind the crystal to 1 and also normalize the width of Figs. 18(a) to 18(c) along the y direction to 1. Figure 19 shows the E^2 distribution along the y direction at the location of the maximum in propagation direction of the ideal case [Fig. 18(a)].

Since light passes through the FOVE, the device's transmittivity becomes also an issue. Sakoda et al.[15] analyzed the wavelength-dependent transmittivity of light, showing that the thickness of crystals and angle of illumination are important factors. In reality, photonic crystals have boundaries with air and the optical behavior caused by the surfaces is considered to be different from that in the middle of the crystal. The influence of the surfaces has been studied by Baba et al.[16] and a method of structural modification was introduced at the crystal surface to improve transmittivity.

Last but not least, the temperature dependence of materials composing a photonic crystal causes a temperature dependence of the crystal's optical behaviors; thus, temperature conditions of the photonic crystals must be taken into consideration when materials for fabrication are determined.

6 Conclusion

We presented the fundamental concept of the FOVE together with the analysis of the negative refractive behavior of photonic crystals. The optical behavior of a photonic crystal designed for this purpose was predicted by investigating the crystal's dispersion characteristics. This prediction was confirmed by rigorous electromagnetic computations using the FMM. The working performance of FOVE was visualized by the ray-trace method, and the sample calculation of the influence of light modulation for data transmission showed that the performance is still valid at

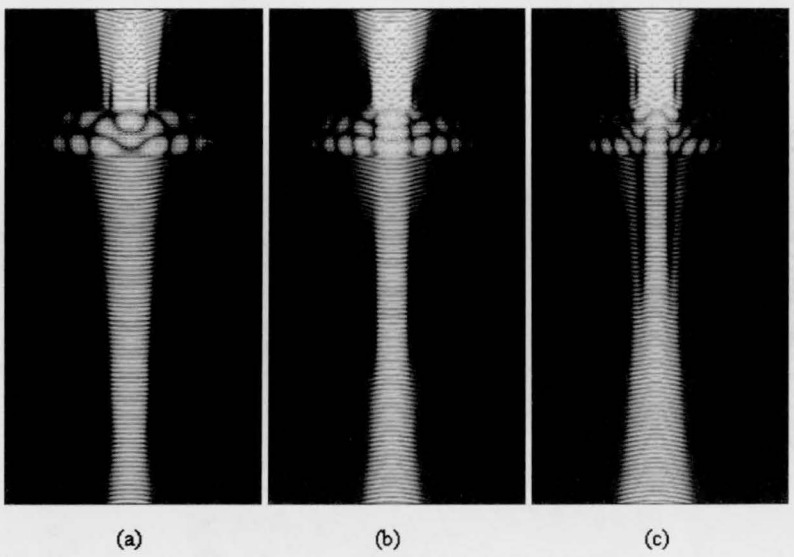

Fig. 18 Snap shots of the square of the electric field (E^2), where (a) represents the ideal alignment, and (b) and (c) represent $\Delta_{max}=0.3$ and $\Delta_{max}=0.5$, respectively.

intensity modulation of RZ and NRZ up to 100 Gbits/s. To obtain an efficiently bent crystal surface, a slight modification was introduced in the crystal's structure. In conjunction with the analysis on the impact of such a deformation to the dispersion diagrams, the propagation behavior of light was computed by the FDTD method. This calculation helped us to visualize the propagation of light through the crystal and also indicated that the approach of the modified crystal structure is useful in designing the FOVE boundary at arbitrary inclination angles.

References

1. M. Toyoshima and K. Araki, "In-orbit measurements of short term attitude and vibrational environment on the Engineering Test Satellite VI using laser communication equipment," *Opt. Eng.* **40**(5), 827–832 (2001).
2. R. K. Tyson, *Principles of Adaptive Optics*, Academic Press, New York (1998).
3. J. D. Joannopoulos, R. D. Meade, and J. N. Winn, *Photonic Crystals: Modeling the Flow of Light*, Princeton University Press, Princeton, NJ (1995).
4. S. G. Johnson, S. Fan, P. R. Vileneuve, and J. D. Joannopoulos, "Guided modes in photonic crystal slabs," *Phys. Rev. B* **60**(8), 5751–5758 (1999).
5. H. Kosaka, T. Kawashima, A. Tomita, M. Notomi, T. Tamamura, T. Sato, and S. Kawakami, "Self-collimating phenomena in photonic crystals," *Phys. Rev. B* **58**(16), R10096–R10099 (1998).
6. B. Gralak, S. Enoch, and G. Tayeb, "Anomalous refractive properties of photonic crystals," *J. Opt. Soc. Am. A* **17**(6), 1012–1020 (2000).
7. Y. Takayama, W. Klaus, and K. Shinohara, "Modified design of photonic crystals with negative refractive behavior to expand the field-of-view of optical receivers," *Proc. SPIE* **5360**, 347–354 (2004).
8. J. Turunen, "Diffraction theory of microrelief gratings," in *Microoptics*, H. P. Herzig, Ed., pp. 31–52, Taylor & Francis, London (1997).
9. A. Taflove and S. C. Hagness, *Computational Electrodynamics the Finite-Difference Time-Domain Method*, Artech House, Boston (2000).
10. J. B. Pendry, "Negative refraction makes a perfect lens," *Phys. Rev. Lett.* **85**(18), 3966–3969 (2000).
11. K. Busch and S. John, "Photonic band gap formation in certain self-organizing systems," *Phys. Rev. E* **58**(3), 3896–3908 (1998).
12. R. D. Meade, A. M. Rappe, K. D. Brommer, J. D. Joannopoulos, and O. L. Alerhand, "Accurate theoretical analysis of photonic-band gap materials," *Phys. Rev. B* **48**(11), 8434–8437 (1993).
13. K. M. Ho, C. T. Chan, and C. M. Soukoulis, "Existence of a photonic gap in periodic dielectric structures," *Phys. Rev. Lett.* **65**(25), 3152–3155 (1990).
14. Y. Takayama, W. Klaus, and K. Shinihara, "Influence of structural misalignment on the negative refractive behavior of photonic crystals," in *Proc. MicroOptics Conf.*, Vol. 10, p. L-50, Elsevier GmbH, Jena, Germany (2004).
15. K. Sakoda, M. Sasada, T. Fukushima, A. Yamanaka, N. Kawai, and K. Inoue, "Detailed analysis of transmission spectra and Bragg-reflection spectra of a two-dimensional photonic crystal with a lattice constant of 1.15 μm," *J. Opt. Soc. Am. B* **16**(3), 361–365 (1999).
16. T. Baba and M. Nakamura, "Photonic crystal light deflection devices using the superprism effect," *IEEE J. Quantum Electron.* **38**(7), 909–914 (2002).

Yoshihisa Takayama received his PhD degree in electronics and information engineering from Hokkaido University, Sapporo, Japan, in 1998. Since 1999 he has been with the National Institute of Information and Communications Technology, Tokyo, Japan. His current research interests are photonic crystals, computational electromagnetics, and free-space laser communications.

Werner Klaus received his MS degree in communications engineering from the Vienna University of Technology, Austria, in 1991 and his PhD degree in electronics engineering from the University of Tokyo, Japan, in 1995. From 1995 to 1997 he was a postdoctoral fellow with the Department of Space Communications, the National Institute of Information and Communications Technology, Japan. Since 1997 he has been a member of the permanent staff at the National Institute of Information and Communications Technology working in the fields of free-space laser communications and micro-optics.

Keisuke Shinohara received his BS, MS, and PhD degrees in engineering science form Osaka University, Japan, in 1994, 1996, and 1998, respectively. In 1998 he joined Fujitsu Laboratories Ltd. as a research fellow of the Japan Society for the Promotion of Science for Young Scientists, working on research and development of high-frequency devices such as InP-based high-electron-mobility transistors (HEMTs). In 1999 he joined Communications Research Laboratory (CRL), where he developed millimeter- and submillimeter-wave devices. In 2004 he joined Rockwell Scientific Company LLC, where he has been engaged in research on high-speed compound semiconductor devices.